Melanoma-secreted lysosomes trigger monocyte-derived dendritic cell apoptosis and limit cancer immunotherapy

Nadine Santana-Magal[1], Leen Farhat-Younis[1], Amit Gutwillig[1], Annette Gleiberman[1], Diana Rasoulouniriana[1], Lior Tal[1], Dvir Netanely[2], Ron Shamir[2], Rachel Blau[3], Meora Feinmesser[1,4], Oran Zlotnik[5], Haim Gutman[5], Ian L. Linde[6], Nathan E. Reticker-Flynn[6], Peleg Rider[1], and Yaron Carmi[1,7]

[1] Department of Pathology, Sackler School of Medicine, Tel Aviv University, Israel

[2] Blavatnik School of Computer Science, Tel Aviv University, Israel

[3] Department of Physiology, Sackler School of Medicine, Tel Aviv University, Israel

[4]Institute of Pathology, Rabin Medical Center – Beilinson Hospital, Petach Tikva, Israel

[5]Department of Surgical Oncology Unit, Rabin Medical Center-Belinson Campus, Petach Tikva, Israel

[6]School of Medicine, Department of Pathology, Stanford University, Palo Alto, California, USA

[7]Corresponding authors:

Yaron Carmi (yaron.carmi@gmail.com)
The Department of Pathology, Sackler School of Medicine, Tel Aviv University, Tel Aviv 69978, Israel. Tel: +972-36409504.

Running title: TIDC are required for anti-tumor T cell activity

keywords: Immunotherapy; cytotoxic T cells; Melanoma; dendritic cells

Conflict of interest: All the authors have declared that no conflict of interest exists

Grant Support:
This work was funded by the SwissBridge Foundation, the Israel Cancer Association (Grant Number 20180041), and the Israel Science Foundation (ISF) (Grant Number 2262/18).

Abstract

The recent success of checkpoint blockade therapies has established immunotherapy as one of the most promising treatments for melanoma. Nonetheless, a complete curative response following immunotherapy is observed only in a fraction of patients. To identify what factors limit the efficacy of immunotherapies, we established mouse models that cease to respond to immunotherapies once their tumors exceed a certain stage. Analysis of the immune systems of the organisms revealed that the numbers of tumor-infiltrating dendritic cells (TIDC) drastically decreased with time. Further, in contrast to the current paradigm, once melanoma was established, TIDC did not migrate into sentinel lymph nodes. Instead, they underwent local cell death due to excessive phagocytosis of lysosomes. Importantly, TIDC were required to license the cytotoxic activity of tumor $CD8^+$ T cells, and in their absence, T cells did not lyse melanoma cells. Our results offer a paradigm shift regarding the role of TIDC and a framework to increase the efficacy of immunotherapies.

Significance

This work redefines the role of monocyte-derived dendritic cells in melanoma and provides a novel strategy to increase the efficacy of T cell-based immunotherapies in non-responding individuals.

Introduction

Patients with advanced melanoma have very poor prognosis and must undergo a series of excruciating treatments of chemotherapy, oncogene inhibitors or combined therapy (1). A number of seminal papers have established a direct correlation between a high frequency of cytotoxic T cells in the tumor mass and improved clinical outcomes (2, 3). As a result, many recent and ongoing clinical trials have attempted to harness the cytotoxic capabilities of T cells to eradicate melanoma. Pioneering therapies based on *de novo* expansion of tumor-infiltrating cytotoxic T cells and their reinfusion to the patient demonstrated the capability of the immune system to mediate tumor rejection (4, 5). Recently, clinical responses were observed in melanoma patients treated with blocking antibodies directed against suppressive receptors on T cells (6, 7). Nonetheless, a complete curative response is observed in only a fraction of the patients, emphasizing the need to improve immunotherapies (8, 9). Given the high mutational rate in melanoma, it is somewhat surprising that the host does not generate an effective T-cell immunity against the tumor cells (10). The general convention suggests that the capacity of tumor cells to edit their presented antigen and their ability to promote a suppressive microenvironment is what restricts the number of melanoma-infiltrating cytotoxic T cells with a limited T cell receptor (TCR) repertoire (11-14).

One way to increase the prevalence of tumor-reactive T cells is through exploiting the antigen presentation capacities of dendritic cells (DC) and their ability to activate cytotoxic T cells (15). DC are composed of heterogeneous cell populations that differ in their morphology, membrane receptors, tissue distribution, migratory and antigen presentation capabilities (16-18). The current understanding of DC ontogeny suggests that they are comprised of four main subsets consisting of plasmacytoid DC (pDC), classical DC type 1 (cDC1), classical DC 2 (cDC2) and monocyte-derived DC (MoDC) (18). While some DC subsets such $CD103^+/CD141^+$, or $CD8^+$ cDC are superior antigen presenting cells, their prevalence in tumors and blood is limited (19, 20). Vaccination with MHC-I and II neo-antigens following resection of stage-IIb/c melanoma lesions can prevent tumor recurrence in human patients (21, 22). However, to date, attempts to employ DC to eradicate established melanoma immunity have shown disappointing results in clinical settings (23).

By mapping the molecular mechanism that regulates the processing of tumor-binding antibodies by DC, we recently generated one of the most potent DC-based immunotherapies for cancer in mice (24, 25). Interestingly, while this treatment has proven effective when tumors were under 20 mm^2, it was almost inert once tumors exceeded an average size of about 40 mm^2. Examination of most reported immunotherapies in mouse melanoma models

(e.g. *ret*, B16F10 and $Braf^{V600E}/PTEN^{-/-}$) indicated that they are limited to early-stage and relatively small tumors (19, 26-30).

We leveraged the unresponsiveness of large tumors to model melanoma patients who do not respond to immunotherapies. We found that in contrast to the current paradigm, melanoma-infiltrating MoDC do not migrate into sentinel lymph nodes, but rather are required *in situ* to license the cytotoxic activity of $CD8^+$ T cells. We further demonstrated that MoDC undergo apoptosis resulting from their uptake of melanoma-secreted lysosomes, and their absence limits the efficacy of immunotherapies. While these models do not fully recapitulate the complexity of the human disease, the principle underlying their capacity to evade immune pressure may be applicable to the human disease.

Material and Methods

Mice

Wild-type (WT) C57BL/6 mice were obtained from Envigo (Jerusalem, Israel). B6;129S-Gt(ROSA)26Sortm1.1(CAG-COX8A/Dendra2)Dcc/J mice were purchased from Jackson Laboratories (Bar-Harbor, ME, USA). B6.Cg-Ptprca Tg (UBC-PA-GFP)1Mnz/J mice were obtained from Dr. Ziv Shulman ,Weizmann Institute, Israel. CD11C-DTR mice were obtained from Prof. Jakub Abramson , Weizmann Institute, Israel. NLRP3 knockout mice were obtained from Prof. Neta Erez at Tel Aviv University, Israel. All mice were housed in an American Association for the Accreditation of Laboratory Animal Care–accredited animal facility and maintained under specific pathogen-free conditions. Animal experiments were approved and conducted in accordance with Tel-Aviv University Laboratory Accreditation #01-16-095. Male and female 8-12 weeks old mice were used in all experiments.

Cell lines

B16F10 (CRL-6475) and YUMM 1.7 (CRL-3362) cells were purchased from ATCC, in January 2017, and *Ret* melanoma cells were a kind gift from Prof. Neta Erez from Tel Aviv University. *Ret* authentication was verified using genome sequencing of enzymes in the MAPK pathway. A375 cell line was a kind gift from Prof. Tamar Geiger from Tel Aviv University. A375 authentication was performed at the Genomics Core Facility of BioRap Technologies and the Rappaport Research Institute in Technion, Israel. Short tandem repeat (STR) profiles were determined using the Promega PowerPlex 16 HS kit. HEK-293FT were purchased from ThermoFisher Scientific (Waltham, MA) in January 2017. Cells were cultured in DMEM supplemented with 10% heat-inactivated FBS, 2 mM L-glutamine, and 100 µg/mL penicillin/streptomycin (all from Biological Industries, Israel). YUMM 1.7 were cultured in DMEM:F12 complete medium. Melan-A cells were purchased from Welcome Trust Functional Genomics Cell Bank, London, UK in February 2019 and were supplemented with 200 nM of Phorbol 12-myristate 13-acetate (PMA) (Santa-Cruz biotechnology, Ca). Primary keratinocytes were a kind gift from Dr. Chen Luxemburg**,** Tel Aviv University, and were cultured as described in (31). All cells were routinely tested for mycoplasma (EZ-PCR Mycoplasma Test Kit, Biological Industries, Israel).

In vivo tumor models

For melanoma tumor studies, $2x10^5$ of B16F10 or YUMM1.7, or $5x10^5$ *ret* cells were suspended in 50 μL of medium and were injected s.c. to C57BL/6 mice above the right flank. The size of growing tumors was measured twice a week using calipers. When tumors reached 200 mm^2, the mice were sacrificed due to ethical considerations.

DC and T cell isolation

All tissue preparations were performed simultaneously from each individual mouse (after euthanasia by CO_2 inhalation). Peripheral blood was collected through perfusion of the right atrium of the heart (HBSS with 10 mM EDTA) into a sodium heparin-coated vacuum tube. Mononuclear cells were collected following centrifugation on Histopaque-1077 Hybri-Max (Sigma Aldrich, Merck, Israel) density gradient medium.

Spleen and LN were homogenized in 2% FBS and 5 mM EDTA supplemented HBSS through 70 μM strainer (ThermoFisher Scientific, Waltham, MA). Tumors were digested in RPMI 1640 with 2 mg/mL collagenase IV, 2,000 U/mL DNase I (both from Sigma Aldrich, Merck, Israel), and 50 ng/mL GM-CSF (Peprotech, Rocky Hill, NJ) for 40 min at 37°C with magnetic stirrers (200 rpm). $CD11b^+$ cells were isolated using magnetic CD11b MicroBeads and column (both from Miltenyi Biotec), incubated for 2 hours in complete RPMI 1640 in 37°C and loosely adhered cells were sorted by FACSAriaII as $FSC^{low}SSC^{low}$ cells.

For T cell isolation, cells were incubated with anti-CD4 or anti-CD8 magnetic beads (MojoSort™ Nanobeads, BioLegend, Carlsbad, CA) according to the manufacturer's instruction. T cells were cultured in RPMI 1640 supplemented with 1% Pen-Strep, 10% heat-inactivated FBS, 1% Sodium pyruvate, 1% MEM-Eagle non-essential amino acids, 1% Insulin-Transferrin-Selenium (PeproTech, Rocky Hill, NJ), 50 μM β-mercaptoethanol (Sigma-Aldrich, Merck, Israel) and were supplemented with 1,000 IU/mL recombinant murine IL-2 (PeproTech, Rocky Hill, NJ) on tissue culture plates pre-coated with 0.5 μg/mL anti-CD3 antibodies (clone 17A2, Biolegend).

Lentiviral infection

Lentivirus were prepared as described (32), briefly, HEK-293FT cells were transfected with pLVX plasmids containing wasabi, or tdTomato under EF1 promoter together with psPAX2 (a gift from Didier Trono, Addgene plasmid # 12260) and pCMV-VSV-G (a gift from Bob Weinberg, Addgene plasmid # 8454). Media-containing viruses were collected after 24 h and

48 h. For infection, B16 cells were incubated with viruses and 100 ug/mL polybrene (Sigma Aldrich, Merck, Israel) for 30 min followed by 30 min centrifugation before medium was replaced. After three days, cells that expressed wasabi, TRP1-GFP, or tdTomato were sorted by FACSAriaII.

Retroviral infection

Retroviruses were prepared as described (32). Briefly, Platinum E cells (a gift from Prof. Cyril Cohen, Bar-Ilan University) were transfected with 2:1 molar ratio of pMIGII and PCL-Eco plasmids (both were kindly provided by Prof. Dario A. A. Vignali). After 48 h, viruses were centrifuged for 1 hour at 100,000 rcf, and suspended in 1 mL media overnight at 4ºC. Splenic $CD8^+$ T cells were cultured on a plate pre-coated with anti-CD3 (0.5 μg/mL) with IL-2 (1,000 IU/mL). Next, 0.3 mL of concentrated retroviruses were added to every $2x10^6$ $CD8^+$ T cells with 10 μg/mL polybrene. Cells were incubated for 30 min, centrifuged at 500 rcf for 1 hour. Medium was replaced and T cells were cultured for additional three days.

Adoptive T Cell Transfer

mice with 8-10 days B16F10 tumors (average 25 mm^2 in size) were injected with $1x10^6$ gp100-TCR expressing $CD8^+$ T cells (26) per mouse after sublethally-irradiation (600 rad), followed by i.p. injections of 300,000 IU of IL-2 (PeproTech, Rocky Hill, NJ) for four consecutive days. To increase DC viability, prior to $CD8^+$ T cell transfer in late-stage tumors, non-irradiated recipient mice were injected i.p with 80 μg/mouse anti-CD40, and with 1 μg/mouse of recombinant GM-CSF.

Tumor immunotherapy

Mice were injected intratumorally with 80 μg anti-CD40 (clone FGK4.5; BioXCell), 0.2 μg TNFα (BioLegend), and 100 μg/mouse anti-TRP1antibody (clone TA99; BioXCell, West Lebanon, NH). CpG ODN1826 and PolyI:C were injected for three consecutive days (50 and 100 μg, respectively, both from InvivoGen, San Diego, CA). For high-doses experiment, 0.5 μg TNFα, 200 μg anti-CD40, 400 μg anti-TRP1, 100 μg CpG ODN1826 and 200 μg PolyI:C were injected. Checkpoint blockade was conducted as described by Twyman-Saint Victor *et al.* (33) with slight modifications. Briefly, tumor-bearing mice were anesthetized with i.p injection of 100 mg/kg ketamine plus 10 mg/kg xylazine and placed on a tray covered with 4

mm thick lead jig exposing only the rear right leg approximately 30 cm from the beam source. Mice were then irradiated at single dose of 15 Gy using Philips industrial X ray machine (1.1 Gy/min). After 24 hours mice were injected i.p with 100 μg of blocking antibodies against CTLA-4 (clone 9D9, BioXCell) and PD-1 (RMP1-14, BioXCell). In some experiments, T cell egression from lymphoid organs was blocked in mice bearing palpable tumors using daily i.p. injections of one mg/kg FTY720 (Sigma Aldrich, Merck, Israel) prior to injection of anti-TRP1 plus anti-CD40 and TNFα immunotherapy.

DC Depletion

To generate CD11c-DTR BM chimeric mice, lethally-irradiated (9 Gy using γ-irradiator Biobeam7000, ^{137}Cs, 2.6 Gy/min) mice were injected i.v. with $5x10^6$ bone marrow cells, and were challenged with $2.5x10^5$ B16F10 cells three weeks later. For $CD11c^+$ cell depletion, mice were injected i.p with 4 ng/g body weight of diphtheria toxin (D0564; Sigma Aldrich, Merck, Israel) six days after tumor challenge. For monocyte depletion, mice were injected with 100 μg of anti-CCL2 (clone-2H5, BioLegend). After 24 hours, mice were treated with $1x10^6$ splenic $CD8^+$ T cell expressing gp100-reactive TCR and with 300,000 IU IL-2, injected i.p daily.

In vivo BrdU incorporation

Tumor-challenged mice were injected i.p. every day with 1 mg of 5-bromo-2-deoxyuridine (BrdU) in 200 μL PBS. At several time points, mice were euthanized, and single cell suspensions were prepared from tumors and draining lymph nodes. Cells were then stained for lineage markers followed by intracellular staining with FITC-conjugated anti-BrdU antibody according to manufacturer's instructions (BD Pharmingen) and analyzed by flow cytometry.

In vivo photoactivation

PA (photo-activated)-GFP and mito-Dendra2 mice were injected s.c. with $2x10^5$ B16F10 cells above the right and left flanks and allowed to grow for eight days. Tumors were illuminated for five minutes with 405 nM wavelength using 20 mWatt led diode, which was custom built by Thorlabs Inc (NJ, USA). After 24 h, DC from the blood, lymph nodes, spleen, and tumor were isolated and analyzed by flow cytometry.

Immunohistochemistry

For frozen sections, prepared as described (32). For anti-mouse staining, the antibodies used were MHCII (clone M5/114.15.2), CD11c (clone N418), CD11b (cloneM1/70), anti-TCRβ (H57- 597), all from BioLegend. Cleaved Caspase-3 (clone 5A1E) from Cell Signaling technologies and LYVE-1 (clone ALY7) from Invitrogen were used. Nuclei were counterstained with Hoechst 33342 (ThermoFisher Scientific, Waltham, MA). For anti-human staining, the antibodies used were HLA-DR (clone L243), CD11c (clone 3.9), both from BioLegend.

Confocal microscopy

B16-Wasabi, $CD8^+$ T cells and $CD11b^+$ DC were co-cultured on glass-bottom confocal plates (Cellvis, Mountain View, CA) in T-cell medium without IL-2 and incubated overnight under standard conditions. For functional assays, DC were incubated for 30 min with 1:50 diluted FITC-labeled latex beads (Sigma Aldrich, Merck, Israel). DC cells were stained with LysoSensor (L7533, ThermoFisher Scientific, Waltham, MA). For visualization of lysosome trafficking, B16F10 cells were stained with lysotracker (L7526, ThermoFisher Scientific, Waltham, MA) for 30 min in 37°C and washed twice before the addition of 50 x 10^4 MoDC. Images were collected using a Zeiss LSM800 confocal laser scanning microscope and analyzed using ZEN software (Carl Zeiss Microscopy).

In vitro Killing assay

Human $CD8^+$ T cells, MoDC and tumor cells were isolated from human melanoma tissue sample, as well as $CD8^+$ T cells from PB. Mouse $CD8^+$ T cells were isolated from various organs of tumor-bearing mice. $CD8^+$ T cells were co-cultured with tumor cells (10,000 cells per well) with or without $CD11b^+$ DC at a ratio of 1:5:2 (T:E:DC) in a round bottom 96-well plate. After 24 hours, cells were incubated for one hour with biotin-conjugated anti-CD107a (BioLegend) at a 1:100 dilution. Cells were further stained with (BV421)-Streptavidin, (Alexa Fluor 488)- CD45, (Brilliant violet 605)-CD8, Annexin V for 15 min and for two min with Propidium Iodide Solution (all from Biolegend) on ice, and staining levels were analyzed by flow cytometry (CytoFLEX, Beckman Coulter, Lakeview Indianapolis, IA).

Exosome and Lysosome Isolation

For isolation of tumor-secreted lysosomes, B16F10, TRP1-GFP expressing B16F10, Melan-

A and A375 cell lines were cultured for 48 h before DMEM supplemented with 10% heat-inactivated FBS centrifuged at 140,000 rpm for 1 h to deplete bovine-derived exosomes. For isolation of T cells-derived lysosomes, $2x10^7$ $CD8^+$ T cells were isolated from spleen or PB and plated in 10 cm plate pre-coated with anti-CD3 antibodies for 48 h. Supernatants were collected and concentrated using Optima™ XPN ultracentrifuge at 140,000 rpm for 1h, the pellet containing either exosomes or lysosomes was resuspended in 50 μL PBS.

Exosomes SEM imaging

Isolated B16F10 and Melan A melanosomes were adsorbed on formvar/ carbon coated grids and stained with 2% aqueous uranyl acetate. Samples were examined using JEM 1400plus transmission electron microscopy.

Luminescence Intensity of Caspase-3/7

$CD11b^+$ DC isolated from tumor, DLN, or PB were cultured in 96 wells (10,000 cells per well) in full DMEM medium supplemented with 50 ng/mL GM-CSF. For apoptotic activity, PB $CD11b^+$ DC were pretreated for 1 h with 25 μM caspase-1 inhibitor VX-765 (CAS 273404-37-8, Santa Cruz Biotechnology) or 20 μM caspase-3 inhibitor (Z-VAD(OMe)-FMK ,CAS 187389-52-2 Santa Cruz Biotechnology) and incubated with: 50 mg/mL in DMSO synthetic melanin (M0418, Sigma Aldrich, Merck, Israel), or with B16F10 exosomes that were untreated, heat-denatured (56^{o}C, 1 h) or lysosomes depleted (biotin-anti-LAMP-1 and streptavidin-magnetic beads; MojoSort™ Nanobeads, BioLegend, Carlsbad, CA). Cells were visualized by confocal microscope or assayed for caspase activity using Caspase-Glo® 3/7 Assay (Promega) in Synergy H1M plate reader (BioTek, Winooski, VT).

Flow cytometry

Cells were analyzed using flow cytometry (CytoFLEX, Beckman Coulter, Lakeview Indianapolis, IA) and sorted by FACS (BD FACSAria™ III, BD Biosciences, Franklin Lakes, NJ). Datasets were analyzed using FlowJo software (Tree Star). The following mice antigen were used: (Brilliant violet 421)-CD45 (clone 30-F11), (Alexa Fluor 647)-MHCII (clone M5/114.15.2), (Alexa Fluor 594, Brilliant violet 605)- CD11c (clone N418), (Per-CP)-CD11b (cloneM1/70), (Alexa Fluor 488)- CD86 (clone GL-1), (PE-Cy7)- CD103 (clone 2E7), (APC-Cy7)- Ly6C (clone HK1.4), (Brilliant violet 421)-βTCR (clone), (PE)- CD4 (clone RM4-4), (Brilliant violet 605)-CD8 (clone 53-6.7), (Alexa Fluor 488)- CD45 (clone 30-F11), (APC)- NKp46 (clone 29AI.4), (PE/Cy7)- CD19 (clone 6D5), (PE)- B220 (clone RA3-6B2), (Alexa Fluor 488)- CCR7 (clone 4B12), (PE)-MERTK (clone 2B10C42).

For human specific antigens, the following antibodies were used: (Alexa Fluor 488) CD3 (HIT3a), (Alexa Fluor 594) CD4 (RPA-T4), (Allophycocyanin) CD19 (HIB19), (Alexa Fluor 647) CD8 (HIT8a), (Brilliant Violet 650) CD11c (3.9), (Alexa Fluor 647) CD16 (3G8), (PerCp/Cy5.5) CD32 (FUN-2), (Brilliant Violet 421) CD64 (10.1), (Allophycocyanin/Cy7) CD45RO (UCHL1), (Phycoerythrin/Cy7) CD45RA (HI100). All Abs were purchased from BioLegend. Cells were suspended in FACS buffer consisting of HBSS with 2% FCS and 0.05mM EDTA.

Gene analysis of melanoma patients

474 melanoma expression profiles from TCGA's RNA-Seq dataset were downloaded from UCSC XENA's web site (http://xena.ucsc.edu/) together with their associated clinical information. We used the PROMO software suite for importing, preprocessing, analyzing and visualizing the data (http://acgt.cs.tau.ac.il/promo/). Six inconsistent samples were removed based on their phenotype labels. The k-means clustering algorithm was applied to the normalized expression levels of 16 dendritic genes, to partition the 468 remaining melanoma samples into four sample groups. The four sample groups are characterized by different levels of the dendritic expression signature. Survival analysis using a Kaplan-Meier plot and the log-rank test showed that the four clusters represent different 5-year survival risks.

Kaplan-Meier plots of melanoma patients based on expression of CD1c (https://www.proteinatlas.org/ENSG00000158481-CD1C/pathology/melanoma) and CD11c (https://www.proteinatlas.org/ENSG00000140678-ITGAX/pathology/melanoma) proteins were calculated from data at the Human Protein Atlas repository (http://www.proteinatlas.org).

Statistical analyses

Each experiment was performed three times. Each experimental group consisted of at least three mice. For time course experiments, significance was calculated using the nonparametric two-way ANOVA with Tukey's correction for multiple hypotheses. In some cases, Bonferroni-Sidak post-test was performed after two-way ANOVA. For two groups analysis, one-way ANOVA with Dunn's test was performed. The results were analyzed by Prism (GraphPad Software, Inc.). All statistical analyses were performed in Prism (GraphPad Software, Inc.)

Study approval

All mice were housed in an animal facility accredited by the American Association for the Accreditation of Laboratory Animal Care and were maintained under specific pathogen–free conditions. Animal experiments were approved and conducted in accordance with Tel Aviv University Laboratory Accreditation (01-17-067 and 01-19-034). The Tel Aviv University Institutional Review Board and Rabin Medical Center – Beilinson board approved the human subject protocols (Helsinki ethical approval 0326-18), and informed consent was obtained from all subjects prior to participation in the study.

Author contributions

NSM has conducted the majority of the experiments and helped to design them. LT, AG, DR, AG, and LFY have conducted some of the experiments. ILL and NRF have conducted photoconverison experiments in dendra2 mice. RB has hepled with isolation and size analyses of tumor-secreted exosomes. MF, OZ, and HG have provided biological materials from human melanoma patients. DN and RS analyzed the melanoma pateints datasets. PR and YC have designed and conducted the experiments and have written the manuscript.

Results

Immunotherapy fails to eradicate late-stage melanoma tumors

Initially, we sought to determine the exact time point at which immunotherapies lose their therapeutic efficacy. To this end, we injected C57BL/6 mice subcutaneously (s.c.) with B16F10 cells and allowed to grow until they reached a palpable size. At several time points, we injected the mice intratumorally with a combination of TNFα+anti-CD40 and antibody against the melanoma antigen TRP1, which was shown to be highly effective in mouse tumors (25, 34). Mice treated until day ten had a significant tumor regression. This treatment was still effective when tumors were treated on day 12, although less potent compared to earlier days. In contrast, this treatment had no impact on tumor size when tumors were treated on day 14, or later (Fig. 1A). Similar results were also obtained using a cell line isolated from *ret* transgenic mice. Injection of TNFα+anti-CD40 and anti-TRP1 antibody to mice bearing tumors under 20 mm^2 induced significant tumor regression, while treating mice bearing large tumors was almost inert (Fig. 1B). Importantly, increasing the dosage of the administrated immunotherapy did not improve the responsiveness of late-stage tumors (Supplementary Fig. S1A-S1B).

We next tested whether this characterizes other immunotherapies, or rather is limited to this particular treatment. Mice bearing B16F10 tumors were injected with TLR9 and TLR7 agonists. Again, treatment efficacy was almost completely abrogated once in late stage tumors (Fig. 1C). Increasing the administrated dosage failed to induce tumor regression in late-stage tumors (Supplementary Fig. S1C). Recently, Twyman-Saint Victor et al. have developed a protocol combining high-dose radiation and checkpoint blockade (33). Injection of antibodies against PD-1 and CTLA-4 followed by local tumor radiation, induced significant tumor regression in small tumors, but not in late-stage tumors (Fig. 1D).

Next, we tested whether adoptive transfer of splenic $CD8^+$ T cells infected with TCR against the melanoma antigen gp100 were injected, along with high-dose IL-2, to sublethally irradiated tumor-bearing mice, according to established protocol (Fig. 1E) (26). Similarly, injection of gp100-reacive T cells induced remarked regression of early-stage tumors, but was almost inert when administrated to mice bearing late-stage tumors (Fig. 1F).

The prevalence of tumor-infiltrating DC is reduced during melanoma progression

We characterized the changes in the composition of immune cell subsets from early to late stage melanoma tumors. We found a drastic reduction over time in the numbers and

percentages of total leukocytes infiltrating B16F10 and *ret* melanoma tumors (Fig. 2A-2C). This reduction was found across almost all immune cell populations, but mainly in NK cells, T cells and DC (Supplementary Fig. S2A-S2B). This reduction was limited to the tumors and was not observed in the blood or draining lymph nodes (DLN) (Supplementary Fig. S2C-2D). While reduction of NK and $CD8^+$ T cells in late-stage tumors is expected to correlate with reduced tumor lysis, why the decrease of tumor-infiltrating DC affects the efficacy of immunotherapy is not clear.

Therefore, we initially set to understand why DC decrease over time. Tumor-infiltrating DC (TIDC) were found to be composed of monocyte-derived DC (MoDC) and migratory $CD103^+$ DC (Supplementary Fig. S2E). Both DC subsets were present in early-stage tumors but almost completely absent in late-stage tumors, when immunotherapies are not effective (Fig. 2D-2E and Supplementary Fig. S2F). Although $CD103^+$ DC are thought to be better antigen-presenting cells, over 90 percent of TIDC are MoDC, providing rationale to further elucidate their impact on the efficacy of immunotherapy. The drastic reduction in MoDC numbers in late-stage tumors was further visualized by tissue sections of mouse melanoma tumors. Sections from day-eight tumors were heavily infiltrated with $CD11b^+$ MoDC, whereas sections from day 14 contained only negligible amounts of MoDC (Fig. 2F).

The general wisdom suggests that following tumor antigen uptake, MoDC migrates to the DLN, to activate T cells. MoDC isolated from wasabi-labeled tumors were found to contain tumor antigens (Fig. 2G), and histological sectioning of these tumors indicated that they are mainly localized in the T-cell zone in the DLN (Supplementary Fig. S2G). Consistently, T-cell numbers in the DLN continued to proliferate throughout tumor progression (Supplementary Fig. S2H) and blocking T-cell egression from lymphoid organs using the sphingosine analog FTY720 almost completely abrogates the therapeutic effect of immunotherapy (Fig. 2H). These results suggest the DLN as the primary site of antigen presentation and the main source for tumor-reactive T cells.

Tumor-infiltrating DC do not migrate into sentinel lymph nodes

Intriguingly, we did not observe any significant increase in the percentages and numbers of MoDC in the DLN or in the blood during tumor progression (Fig. 3A-3B and Supplementary Fig. S3A-3C). Additionally, all the tumor lymph vessels are located in the tumor periphery, with no lymph vessels penetrating the center of the tumors, where the majority of MoDC are. All DC adjacent to or inside lymph vessels have expressed low levels of CD11c and Ly6C,

suggesting that they are dermal DC or Langerhans cells, and not MoDC (Fig. 3C). We could also detect secreted tumor antigens, such as TRP1, in MoDC found in DLN, suggesting that tumor antigens can be passively drained (Supplementary Fig. S3D-S3E). Additionally, MoDC did not express detectable levels of CCR7, which is required for their migration to the DLN (Fig. 3D).

To monitor migration patterns of MoDC we used mice expressing the green-to-red photoconvertible fluorescent protein Dendra2. Mice were injected s.c. with B16F10 cells, and tumors were allowed to grow for eight days. We then performed a small surgery on the skin adjacent to the tumor and tumor was illuminated using a 405 nm diode LED array (Fig. 3E). After 24 hours, blood, spleen, tumor, right inguinal DLN and left axillary non-DLN were removed, and the green-red conversion in MoDC was analyzed by flow cytometry. We could not detect MoDC expressing red fluorescence protein in any of the tested organ, but the tumors (Fig. 3F-3G). In contrast, B cells, NKT cells, and neutrophils expressing red fluorescence protein were found in the blood and lymphoid tissues across the body (Supplementary Fig. S3F). One caveat to this method is the relatively rapid decaying of red fluorescence signal, as immediately after illumination, about 80 percent of immune cells expressed red fluorescence whereas after 24 hours about 40 percent remained positive (Supplementary Fig. S3G). Therefore, we also used mice expressing photoactivatable GFP protein (PA-GFP), which is more stable compared to Dendra2, but has a much lower fluorescence intensity. We could detect $CD103^+$ DC and monocytes, but not in mature MoDC, expressing PA-GFP in DLN of tumor-bearing mice (Fig. 3H-3I).

Tumor-infiltrating DC undergo inflammasome-mediated cell death due to uptake of tumor-secreted lysosomes

When isolating MoDC from tumors we noticed that MoDC from late-stage tumors, but not early-stage tumors, exhibit rapid cell death when cultured *in vitro* (Fig. 4A). Caspase 3/7 activity assay indicated that these cells undergo apoptosis (Fig. 4B). In contrast, MoDC isolated from the DLN and blood of late-stage tumor-bearing mice were viable and comparable to MoDC from early-stage tumors and naïve mice (Fig. 4A-4B). While MoDC from late-stage tumors, have completely lost their ability to phagocytize latex beads, the phagocytotic capacity of MoDC from early-stage tumors were comparable to that of naïve mice (Supplementary Fig. S4A). Consistently, higher levels of cleaved caspase-3 were

observed in histological sections of late-stage tumors, in comparison to early-stage sections (Fig. 4C).

We also noticed that most tumor-infiltrating MoDC, even in early-stage tumors, contain a high density of melanosomes, indicative of exosomes uptake (Supplementary Fig. S4B). Therefore, we isolated exosomes from the supernatants of B16F10 cells and incubated them with MoDC from the blood of tumor-bearing mice. As a control, we used synthetic melanin, or melanosomes isolated from immortalized melanocytes (Fig. 4D). Incubation with exosomes from B16F10, but not from normal melanocytes or with melanin, induced massive apoptosis of MoDC (Fig. 4E and Supplementary Fig. S4C). Induction of apoptosis by exosomes was limited to MoDC, as incubation of primary keratinocytes and splenic T cells with melanoma-secreted exosomes did not induce their apoptosis (Supplementary Fig. S4D). Analysis of B16 mutanome indicated that none of the enzymes that synthesize melanin are mutated in B16F10 (35). Furthermore, the examination of B16F10 melanosomes under electron microscopy indicated that they are intact and similar to the melanosomes secreted from normal melanocytes (Supplementary Fig. S4E), suggesting that other exosomes may be involved. In addition to melanosomes, B16F10 secrete also high levels of lysosomes (Supplementary Fig. S4F). Selective labeling of lysosomes in B16F10 indicated that they are efficiently taken up by MoDC (Supplementary Fig. S4G). Depleting the lysosomes from melanoma-derived exosomes prior to incubation with MoDC almost completely prevented apoptosis (Fig. 4F-4G).

Denaturation of melanoma-secreted exosomes at 56^{o}C for 30 minutes prior to their incubation with MoDC completely blocked their capacity to induce apoptosis (Fig. 4F-4G). Incubation of MoDC with a pan-caspase inhibitor – or with VX-765, a selective inhibitor of caspases 1 and 4 – significantly inhibited apoptosis in these cells (Fig. 4F-4G and Supplementary Fig. S4H). Consistently, apoptosis induced by lysosomes was almost completely abrogated in MoDC obtained from mice deficient in Nod-like receptor protein 3 (NLRP3 KO) (Fig. 4H-4I). Lysosomes isolated from splenic T cells induce apoptosis in MoDC at levels similar to that induced by melanoma-secreted lysosomes (Fig. 4H), suggesting that this is not a result of a special feature of melanoma-derived lysosomes.

Next, we tested the effectivity of immunotherapy in late-stage melanoma that do not secrete lysosomes. Screening analysis indicated that YUMM1.7 melanoma cells (36) do not secrete lysosomes (Supplementary Fig. S4H). Thus, mice bearing large tumors were treated with combination of TNFα+anti-CD40 and anti-TRP1 antibodies. Indeed, these tumors contained

viable MoDC and tumors underwent regression upon administration of immunotherapy (Fig. 4J).

Tumor-infiltrating MoDC are required to license the cytotoxic activity of CD8$^+$ T cells

We next addressed why the absence of tumor-infiltrating MoDC affects the outcomes of immunotherapies. Although the DLN is a major site in which tumor-reactive T cells are generated, incubation of CD8$^+$ T cells isolated from the blood, or DLN of B16F10 tumor-bearing mice with B16F10 cells did not result in release of lytic granules and tumor cell lysis (Fig. 5A-5C). In sharp contrast, incubation of B16F10 cells with day eight tumor-infiltrating CD8$^+$ T cells resulted in significant lysis of B16F10 cells and secretion of lytic granules from T cells (Fig. 5A-5C). Addition of MoDC isolated from the tumor, but not from the blood or the DLN of tumor-bearing mice, induced the release of cytotoxic granules from CD8$^+$ T cells and tumor cell lysis (Fig. 5D-5F). Consistent with their loss of function, MoDC from late-stage tumors failed to promote secretion of lytic granules and tumor cells lysis by CD8$^+$ T cells (Supplementary Fig. S5A).

We next tested whether the signals that induce CD8$^+$ T-cell activation are secreted by MoDC, or rather are cell-contact dependent. Thus, CD8$^+$ T cells from the DLN of tumor-bearing mice were incubated with B16F10 cells in the presence of the isolated DC or with their supernatants. Significant tumor cell lysis and secretion of lytic granules over baseline levels were observed only upon addition of tumor-infiltrating MoDC, but not their supernatants, indicating that T cell activation required cell contact (Fig. 5G-5H and Supplemental Data, Fig. 5B). CD8$^+$ T cell activation was not reduced upon blocking of MHCI-TCR interactions (Fig. 5I).

Since MoDC express higher levels of CD86 and CD40 (Fig. 5J-5K), we tested whether stimulation of MoDC with classical adjuvants is sufficient to activate CD8$^+$ T cells. Thus, peripheral blood MoDC were isolated and activated with LPS, or ant-CD40 and added to a co-culture of CD8$^+$ T cells and tumor cells. Similarly to MoDC from tumors, stimulated blood MoDC activated CD8$^+$ T cells to secrete lytic granules and to kill tumor cells (Fig. 5L-5M).

Tumor-infiltrating MoDC are required for CD8$^+$ T cells immunotherapy

To test whether tumor MoDC are indeed required for T cell immunity, we generated CD11c-DTR BM chimeric mice and challenged them with B16F10 cells. Once tumor reached a palpable size, mice were injected with diphtheria toxin to systemically deplete DC followed by adoptive transfer of gp100-reactive T cells. While injection of T cells to tumor-bearing control mice induced tumor regression, their administration to DC-depleted mice was almost inert (Fig. 6A). Since depletion of CD11c is not restricted to MoDC, we next tested if blocking monocyte migration will affect T cell immunotherapy. Mice bearing palpable B16F10 tumors were treated with anti-CCL2 antibodies followed by adoptive transfer of gp100-reactive T cells, or intertumoral injections of TNFα+anti-CD40 and anti-TRP1 antibodies. In both experiments, blocking monocyte migration significantly reduced the efficacy of the administrated immunotherapies (Fig. 6B-6C).

We also tested whether increasing the viability and activity of MoDC in late-stage tumors will improve the efficacy of tumor-reactive $CD8^+$ T cells. Mice were injected with B16F10 and tumors were allowed to grow for at least ten days, until they reached an average size of 50 mm^2, when adoptive transfer of $CD8^+$ T cells is no longer effective. Mice were then treated with gp100-reactive $CD8^+$ T cells alone, or in combination with anti-CD40 and GM-CSF, which we found to increase MoDC numbers and viability in tumors (Fig. 6D-6E). The effect of $CD8^+$ T cells alone, or in combination with GM-CSF was benign and did not reduce tumor burden. In sharp contrast, injection of T cells in combination with anti-CD40, with or without GM-CSF, induced significant tumor regression (Fig. 6F).

Human melanomas induce apoptosis of MoDC and correlate with poor clinical outcomes

We next sought to determine if these finding are also applicable to human melanoma patients. Initially, we assessed whether a gene expression signature of activated MoDC correlates with improved survival of melanoma patients. We performed an unsupervised analysis of gene expression profiles of 468 melanoma patient samples obtained from The Cancer Genome Atlas (TCGA) repository (37) using PROMO software tool (http://acgt.cs.tau.ac.il/promo/). Patient's profiles were clustered into four groups, based on the expression levels of 16 genes associated with activated MoDC (Fig. 7A). Kaplan-Meier plot of these four groups indicated a direct correlation between the activated MoDC and improved survival (Fig. 7B). While the gene signature of activated MoDC may correlate with other immune subsets, this analysis highlights their prevalence as a predictive prognostic marker. Additionally, dataset analysis of melanoma patients from the Human Protein Atlas repository indicated that proteins

predominantly expressed on myeloid DC correlate with improved survival of melanoma patients (Supplementary Fig. S6A-S6B).

To test if MoDC are needed to license the cytotoxic activity of tumor-reactive T cells, tumor cells from a melanoma patient were incubated with autologous T cells isolated from the tumor, and peripheral blood. Tumor-infiltrating T cells induced apoptosis in about 15 percent of tumor cell, while blood T cells were almost inert. Addition of autologous tumor-infiltrating MoDC ($SSC^{lo}/MHCII^{hi}/CD11c^{+}/CD14^{lo\text{-}int}$) to the blood T cells promoted tumor cells killing comparable to that observed with tumor-infiltrating T cells (Fig. 7C-7D).

Histological sections of primary melanoma from patient resistant to PD-1 treatment showed high levels of cleaved caspase 3 in the majority of tumor-infiltrating DC (Fig. 7E). Finally, Consistent with our results in mice, exosomes secreted from melanoma cell line were found to induced apoptosis in MoDC isolated from healthy donors (Fig. 7F-7G).

Discussion

While immunotherapies for melanomas have been proven effective even in disseminated and metastatic disease (4, 9), only a small subset of patients experience a complete curative response (8). Therefore, a huge scientific effort has been invested into identifying the factors that limit treatment efficacy. Several meta-analysis studies of clinical samples have attempted to identify a gene signature that will predict responsiveness of cancer patients to immunotherapies (3, 38). The net parameters that determine whether a patient will respond may depend on the driver mutations, mutational load, antigen presentation machinery, and neoantigen burden (39, 40), as well as on immune parameters in the tumor microenvironment, such as the type, prevalence, cytokine signature, and diversity of TCR of infiltrating T cells (3, 38, 41, 42).

Here, we leveraged the unresponsiveness of large melanoma tumors in mice to immunotherapies, to identify immune elements that govern the host immune response to melanoma. We found that tumor-infiltrating MoDC undergo apoptosis as melanoma progresses; and in their absence, T-cell-based therapies will not work. Examination of clinical biopsies indicated a positive correlation between tumor-infiltrating myeloid and monocyte-derived DC, and favorable clinical outcomes in cutaneous melanomas (20, 43-45). Substantial reduction of DC in the epidermis along tumor progression has been reported starting three decades ago in melanoma patients (43, 44, 46, 47). Esche et al were the first to report that tumor-derived factors induce apoptosis in murine and human DC (48). Attempts to identify which melanoma-derived factor induces DC apoptosis suggested that GM3 and GD3 gangliosides through activation of reactive-oxygen species (49, 50), or MUC2 secreted through ligation to Siglec-3 (51). Notably, this is the first time that melanoma-derived lysosomes are suggested to be the main mechanism that induces apoptosis in MoDC through induction of inflammasome and caspase 1. It remains unclear why up-take of lysosomes by tumor-associated macrophages is not followed by apoptosis.

Most studies attributed the positive correlation between tumor-infiltrating DC and favorable prognosis to the capacity of DC to migrate into sentinel lymph nodes, where they prime tumor-reactive T cells (19, 20, 52-55). We found that MoDC are different than cDC and epidermal DC, as they do not migrate to lymphoid organs, but rather remain in tumors and provide stimulatory signals to tumor-infiltrating T cells. Consistent with the seminal work of Randolph (56), which found that monocytes engulfing latex beads migrate to DLN and mature to become DC, we found monocyte, but not mature MoDC, containing tumor antigens in lymphoid organs. Numerous clinical trials have attempted to pulse *ex vivo* autologous

MoDC with tumor antigens and re-infused them into the patient in order to elicit T-cell immunity (57, 58). Although routes of injections play an important role in facilitating this treatment (59), our work provides another explanation as to why injection of MoDC did not meet expectations by activating T cells in *in vitro* assays.

The exact nature of the licensing signal that tumor-infiltrating MoDC provide to T cells remains unclear. Marigo and colleagues have demonstrated that tumor-infiltrating Tip DC, which is a subset of MoDC, activate the infiltrating T cells through crosslinking of CD40 ligand (60). Nonetheless, since CD40L lacks a signaling chain, it is more likely that they activate the CD40 of Tip-DC and that the licensing signaling is secondary to CD40-CD40L interactions. Indeed, the activation of MoDC with agonistic anti-CD40, which block subsequent interactions with CD40L on T cells, induces significant tumor cell lysis by T cells.

Overall, this work redefines the role of MoDC in melanomas, and potentially in other tumors; it suggests that their main role is not to present tumor antigens in sentinel lymph nodes, but rather to provide *in situ* licensing signals to infiltrating T cells. Improving DC viability in patients who do not respond to immunotherapy may increase treatment efficacy substantially.

Acknowledgements

The authors would like to deeply thanks Rabin Medical Center institutional Tissue Bank and especially Dr. Adva Levi-Barda, for their invaluable support of this research.

References

1. Geller AC, Clapp RW, Sober AJ, Gonsalves L, Mueller L, Christiansen CL, et al. Melanoma epidemic: an analysis of six decades of data from the Connecticut Tumor Registry. *J Clin Oncol.* 2013;31(33):4172-8.
2. Pages F, Galon J, Dieu-Nosjean MC, Tartour E, Sautes-Fridman C, and Fridman WH. Immune infiltration in human tumors: a prognostic factor that should not be ignored. *Oncogene.* 2010;29(8):1093-102.
3. Thorsson V, Gibbs DL, Brown SD, Wolf D, Bortone DS, Ou Yang TH, et al. The Immune Landscape of Cancer. *Immunity.* 2018;48(4):812-30 e14.
4. Rosenberg SA. Decade in review-cancer immunotherapy: entering the mainstream of cancer treatment. *Nat Rev Clin Oncol.* 2014;11(11):630-2.
5. Restifo NP, Dudley ME, and Rosenberg SA. Adoptive immunotherapy for cancer: harnessing the T cell response. *Nat Rev Immunol.* 2012;12(4):269-81.
6. Pardoll DM. The blockade of immune checkpoints in cancer immunotherapy. *Nature reviews Cancer.* 2012;12(4):252-64.
7. Hodi FS, O'Day SJ, McDermott DF, Weber RW, Sosman JA, Haanen JB, et al. Improved survival with ipilimumab in patients with metastatic melanoma. *N Engl J Med.* 2010;363(8):711-23.
8. Sharma P, and Allison JP. The future of immune checkpoint therapy. *Science.* 2015;348(6230):56-61.
9. Postow MA, Callahan MK, and Wolchok JD. Immune Checkpoint Blockade in Cancer Therapy. *J Clin Oncol.* 2015;33(17):1974-82.
10. Hayward NK, Wilmott JS, Waddell N, Johansson PA, Field MA, Nones K, et al. Whole-genome landscapes of major melanoma subtypes. *Nature.* 2017;545(7653):175-80.
11. Joyce JA, and Fearon DT. T cell exclusion, immune privilege, and the tumor microenvironment. *Science.* 2015;348(6230):74-80.
12. Schumacher TN, Scheper W, and Kvistborg P. Cancer Neoantigens. *Annu Rev Immunol.* 2019;37:173-200.
13. Coussens LM, Zitvogel L, and Palucka AK. Neutralizing tumor-promoting chronic inflammation: a magic bullet? *Science.* 2013;339(6117):286-91.
14. Gajewski TF, Schreiber H, and Fu YX. Innate and adaptive immune cells in the tumor microenvironment. *Nature immunology.* 2013;14(10):1014-22.
15. Palucka K, and Banchereau J. Dendritic-cell-based therapeutic cancer vaccines. *Immunity.* 2013;39(1):38-48.
16. Mildner A, and Jung S. Development and function of dendritic cell subsets. *Immunity.* 2014;40(5):642-56.
17. Merad M, Sathe P, Helft J, Miller J, and Mortha A. The dendritic cell lineage: ontogeny and function of dendritic cells and their subsets in the steady state and the inflamed setting. *Annu Rev Immunol.* 2013;31:563-604.
18. Guilliams M, Ginhoux F, Jakubzick C, Naik SH, Onai N, Schraml BU, et al. Dendritic cells, monocytes and macrophages: a unified nomenclature based on ontogeny. *Nat Rev Immunol.* 2014;14(8):571-8.
19. Salmon H, Idoyaga J, Rahman A, Leboeuf M, Remark R, Jordan S, et al. Expansion and Activation of CD103(+) Dendritic Cell Progenitors at the Tumor Site Enhances Tumor Responses to Therapeutic PD-L1 and BRAF Inhibition. *Immunity.* 2016;44(4):924-38.
20. Roberts EW, Broz ML, Binnewies M, Headley MB, Nelson AE, Wolf DM, et al. Critical Role for CD103(+)/CD141(+) Dendritic Cells Bearing CCR7 for Tumor Antigen Trafficking and Priming of T Cell Immunity in Melanoma. *Cancer Cell.* 2016;30(2):324-36.
21. Sahin U, Derhovanessian E, Miller M, Kloke BP, Simon P, Lower M, et al. Personalized RNA mutanome vaccines mobilize poly-specific therapeutic immunity against cancer. *Nature.* 2017;547(7662):222-6.
22. Ott PA, Hu Z, Keskin DB, Shukla SA, Sun J, Bozym DJ, et al. An immunogenic personal neoantigen vaccine for patients with melanoma. *Nature.* 2017;547(7662):217-21.

23. Butterfield LH. Dendritic cells in cancer immunotherapy clinical trials: are we making progress? *Front Immunol.* 2013;4:454.
24. Carmi Y, Prestwood TR, Spitzer MH, Linde IL, Chabon J, Reticker-Flynn NE, et al. Akt and SHP-1 are DC-intrinsic checkpoints for tumor immunity. *JCI Insight.* 2016;1(18):e89020.
25. Carmi Y, Spitzer MH, Linde IL, Burt BM, Prestwood TR, Perlman N, et al. Allogeneic IgG combined with dendritic cell stimuli induce antitumour T-cell immunity. *Nature.* 2015;521(7550):99-104.
26. Overwijk WW, Tsung A, Irvine KR, Parkhurst MR, Goletz TJ, Tsung K, et al. gp100/pmel 17 is a murine tumor rejection antigen: induction of "self"-reactive, tumoricidal T cells using high-affinity, altered peptide ligand. *The Journal of experimental medicine.* 1998;188(2):277-86.
27. Caisova V, Vieru A, Kumzakova Z, Glaserova S, Husnikova H, Vacova N, et al. Innate immunity based cancer immunotherapy: B16-F10 murine melanoma model. *BMC Cancer.* 2016;16(1):940.
28. Fu J, Kanne DB, Leong M, Glickman LH, McWhirter SM, Lemmens E, et al. STING agonist formulated cancer vaccines can cure established tumors resistant to PD-1 blockade. *Sci Transl Med.* 2015;7(283):283ra52.
29. Curran MA, Montalvo W, Yagita H, and Allison JP. PD-1 and CTLA-4 combination blockade expands infiltrating T cells and reduces regulatory T and myeloid cells within B16 melanoma tumors. *Proc Natl Acad Sci U S A.* 2010;107(9):4275-80.
30. Zhu EF, Gai SA, Opel CF, Kwan BH, Surana R, Mihm MC, et al. Synergistic innate and adaptive immune response to combination immunotherapy with anti-tumor antigen antibodies and extended serum half-life IL-2. *Cancer Cell.* 2015;27(4):489-501.
31. Polak D, Zigron A, Eli-Berchoer L, Shapira L, and Nussbaum G. Myd88 plays a major role in the keratinocyte response to infection with Porphyromonas gingivalis. *Journal of periodontal research.* 2019.
32. Rasoulouniriana D, Santana-Magal N, Gutwillig A, Farhat-Younis L, Wine Y, Saperia C, et al. A distinct subset of FcgammaRI-expressing Th1 cells exert antibody-mediated cytotoxic activity. *J Clin Invest.* 2019;129(10):4151-64.
33. Twyman-Saint Victor C, Rech AJ, Maity A, Rengan R, Pauken KE, Stelekati E, et al. Radiation and dual checkpoint blockade activate non-redundant immune mechanisms in cancer. *Nature.* 2015;520(7547):373-7.
34. Spitzer MH, Carmi Y, Reticker-Flynn NE, Kwek SS, Madhireddy D, Martins MM, et al. Systemic Immunity Is Required for Effective Cancer Immunotherapy. *Cell.* 2017;168(3):487-502 e15.
35. Castle JC, Kreiter S, Diekmann J, Lower M, van de Roemer N, de Graaf J, et al. Exploiting the mutanome for tumor vaccination. *Cancer Res.* 2012;72(5):1081-91.
36. Meeth K, Wang JX, Micevic G, Damsky W, and Bosenberg MW. The YUMM lines: a series of congenic mouse melanoma cell lines with defined genetic alterations. *Pigment Cell Melanoma Res.* 2016;29(5):590-7.
37. Cancer Genome Atlas N. Genomic Classification of Cutaneous Melanoma. *Cell.* 2015;161(7):1681-96.
38. Auslander N, Zhang G, Lee JS, Frederick DT, Miao B, Moll T, et al. Robust prediction of response to immune checkpoint blockade therapy in metastatic melanoma. *Nat Med.* 2018;24(10):1545-9.
39. McGranahan N, Furness AJ, Rosenthal R, Ramskov S, Lyngaa R, Saini SK, et al. Clonal neoantigens elicit T cell immunoreactivity and sensitivity to immune checkpoint blockade. *Science.* 2016;351(6280):1463-9.
40. Samstein RM, Lee CH, Shoushtari AN, Hellmann MD, Shen R, Janjigian YY, et al. Tumor mutational load predicts survival after immunotherapy across multiple cancer types. *Nat Genet.* 2019;51(2):202-6.
41. Riaz N, Havel JJ, Makarov V, Desrichard A, Urba WJ, Sims JS, et al. Tumor and Microenvironment Evolution during Immunotherapy with Nivolumab. *Cell.* 2017;171(4):934-49 e16.

42. Hugo W, Zaretsky JM, Sun L, Song C, Moreno BH, Hu-Lieskovan S, et al. Genomic and Transcriptomic Features of Response to Anti-PD-1 Therapy in Metastatic Melanoma. *Cell.* 2016;165(1):35-44.
43. Reichert TE, Scheuer C, Day R, Wagner W, and Whiteside TL. The number of intratumoral dendritic cells and zeta-chain expression in T cells as prognostic and survival biomarkers in patients with oral carcinoma. *Cancer.* 2001;91(11):2136-47.
44. Ladanyi A, Kiss J, Somlai B, Gilde K, Fejos Z, Mohos A, et al. Density of DC-LAMP(+) mature dendritic cells in combination with activated T lymphocytes infiltrating primary cutaneous melanoma is a strong independent prognostic factor. *Cancer Immunol Immunother.* 2007;56(9):1459-69.
45. Goc J, Germain C, Vo-Bourgais TK, Lupo A, Klein C, Knockaert S, et al. Dendritic cells in tumor-associated tertiary lymphoid structures signal a Th1 cytotoxic immune contexture and license the positive prognostic value of infiltrating CD8+ T cells. *Cancer Res.* 2014;74(3):705-15.
46. Stene MA, Babajanians M, Bhuta S, and Cochran AJ. Quantitative alterations in cutaneous Langerhans cells during the evolution of malignant melanoma of the skin. *J Invest Dermatol.* 1988;91(2):125-8.
47. Toriyama K, Wen DR, Paul E, and Cochran AJ. Variations in the distribution, frequency, and phenotype of Langerhans cells during the evolution of malignant melanoma of the skin. *J Invest Dermatol.* 1993;100(3):269S-73S.
48. Esche C, Lokshin A, Shurin GV, Gastman BR, Rabinowich H, Watkins SC, et al. Tumor's other immune targets: dendritic cells. *J Leukoc Biol.* 1999;66(2):336-44.
49. Peguet-Navarro J, Sportouch M, Popa I, Berthier O, Schmitt D, and Portoukalian J. Gangliosides from human melanoma tumors impair dendritic cell differentiation from monocytes and induce their apoptosis. *J Immunol.* 2003;170(7):3488-94.
50. Bennaceur K, Popa I, Chapman JA, Migdal C, Peguet-Navarro J, Touraine JL, et al. Different mechanisms are involved in apoptosis induced by melanoma gangliosides on human monocyte-derived dendritic cells. *Glycobiology.* 2009;19(6):576-82.
51. Ishida A, Ohta M, Toda M, Murata T, Usui T, Akita K, et al. Mucin-induced apoptosis of monocyte-derived dendritic cells during maturation. *Proteomics.* 2008;8(16):3342-9.
52. Spranger S, Dai D, Horton B, and Gajewski TF. Tumor-Residing Batf3 Dendritic Cells Are Required for Effector T Cell Trafficking and Adoptive T Cell Therapy. *Cancer Cell.* 2017;31(5):711-23 e4.
53. Ma Y, Adjemian S, Mattarollo SR, Yamazaki T, Aymeric L, Yang H, et al. Anticancer chemotherapy-induced intratumoral recruitment and differentiation of antigen-presenting cells. *Immunity.* 2013;38(4):729-41.
54. Kuhn S, Hyde EJ, Yang J, Rich FJ, Harper JL, Kirman JR, et al. Increased numbers of monocyte-derived dendritic cells during successful tumor immunotherapy with immune-activating agents. *J Immunol.* 2013;191(4):1984-92.
55. Broz ML, Binnewies M, Boldajipour B, Nelson AE, Pollack JL, Erle DJ, et al. Dissecting the tumor myeloid compartment reveals rare activating antigen-presenting cells critical for T cell immunity. *Cancer Cell.* 2014;26(5):638-52.
56. Randolph GJ, Inaba K, Robbiani DF, Steinman RM, and Muller WA. Differentiation of phagocytic monocytes into lymph node dendritic cells in vivo. *Immunity.* 1999;11(6):753-61.
57. Anguille S, Smits EL, Lion E, van Tendeloo VF, and Berneman ZN. Clinical use of dendritic cells for cancer therapy. *Lancet Oncol.* 2014;15(7):e257-67.
58. Wimmers F, Schreibelt G, Skold AE, Figdor CG, and De Vries IJ. Paradigm Shift in Dendritic Cell-Based Immunotherapy: From in vitro Generated Monocyte-Derived DCs to Naturally Circulating DC Subsets. *Front Immunol.* 2014;5:165.
59. Fong L, Brockstedt D, Benike C, Wu L, and Engleman EG. Dendritic cells injected via different routes induce immunity in cancer patients. *J Immunol.* 2001;166(6):4254-9.
60. Marigo I, Zilio S, Desantis G, Mlecnik B, Agnellini AHR, Ugel S, et al. T Cell Cancer Therapy Requires CD40-CD40L Activation of Tumor Necrosis Factor and Inducible Nitric-Oxide-Synthase-Producing Dendritic Cells. *Cancer Cell.* 2016;30(3):377-90.

Figure Legends

Fig. 1: Immunotherapy fails to eradicate late-stage melanoma tumors. (**A**) Tumor size in mice injected s.c. with B16F10 cells and treated with anti-TRP1 antibodies+ CD40L and TNFα (n=4). (**B**) Tumor size in mice injected with *ret* melanoma cells and treated intratumorally with anti-TRP1+anti-CD40 and TNFα (n=3). (**C**) Tumor size in mice injected with B16F10 cells and treated daily with CpG and PolyI:C. (**D**) Tumor size in mice injected with B16F10 cells, locally irradiated with 15 Gy and treated with anti- CTLA-4 and anti-PD-1. (**E**) Illustration of experimental design. Fig. was created using BioRender (https://biorender.com/). (**F**) Tumor size in mice injected s.c. with B16F10 cells and treated with gp100- reactive $CD8^+$ T cells and high-dose IL-2 (n=4). Shown is one representative experiment out of at least three performed. Statistical significance was calculated using ANOVA with Tukey's correction for multiple comparisons (**denotes $p<0.01$, **** denotes $p<0.0001$).

Fig. 2: The prevalence of tumor-infiltrating DC is reduced during melanoma progression. (**A**) Mean percentages of $CD45^+$ cells infiltrating B16F10 tumors (n=3). **(B)** Mean $CD45^+$ cell counts in B16F10 tumors (n=3). (**C**) Representative CD45 staining in histological sections of B16F10 from early-stage (day 6) and late-stage (day 14) tumors. (**D**) Mean cell count of $CD103^+$ DC and MoDC infiltrating B16F10 tumors over time (n=3). (**E**) Representative flow cytometry analysis of tumor-infiltrating DC in B16F10 tumors from early-stage (day 6) and late-stage (day 14). (**F**) Histological staining of tumor-infiltrating DC in B16F10 tumors on early-stage (day 8) and late-stage (day 14) (x200). (**G**) Confocal images of $CD11b^+$ DC isolated from tumors and DLN of mice challenged with wasabi-labeled B16F10. (**H**) B16F10 tumor size following injection of anti-TRP1+ anti-CD40 and TNFα and with daily injection of FTY720 (n=4). Shown is one experiment out of at least three performed. Statistical significance was calculated using ANOVA with Tukey's correction for multiple comparisons (*** denotes $p<0.001$, **** denotes $p<0.0001$).

Fig. 3: Tumor-infiltrating DC do not migrate into sentinel lymph-nodes. (**A**) Mean percentages of pan DC in B16F10 tumor-bearing mice (n=3). (**B**) FACS analysis of DC in B16F10 tumor-bearing mice on early stage (day 6) and late stage (day 14) (n=3). (**C**) Histological staining of DC and lymphatic vessels in TRP1-GFP labeled B16F10 in day 8 tumors (x200). (**D**) CCR7 expression on DC from day 8 B16F10 tumors. (**E**) Illustration of experimental outline. This Fig. was created using BioRender (https://biorender.com/). (**F**) Mean percentages of Dendra2-expressing MoDC out of $CD11b^+/CD11c^+/MHCII^+$ cells in day 8 tumor-bearing-mice. (**G**) FACS analysis of red Dendra2 expression in. (**H**) Confocal images of $CD11b^+$ cells from B16F10 tumor-bearing PA-GFP mice 24h after tumor illumination. (**I**) Left, mean percentages of tumor-MoDC expressing PA-GFP. Right, representative FACS analysis PA-GFP expression in MoDC. Shown is one experiment out of at least three performed. Statistical significance was calculated using ANOVA with Tukey's correction for multiple comparisons (*** denotes $p<0.001$, **** denotes $p<0.0001$).

Fig. 4: Tumor-infiltrating DC undergo cell death due to uptake of tumor-secreted lysosomes- **(A)** Confocal microscopy of $CD11b^+$ DC sorted from tumor-bearing mice on early-stage (day 8) and late-stage (day 14) (x400). **(B)** Caspase 3/7 activity in DC from tumor-bearing mice on early-stage (day 8) and late-stage (day 14). (**C**) Histological staining of cleaved caspase 3 on early-stage (day 8) and late-stage (day 14) tumors (x200). (**D**) Isolation protocol of melanocytes and melanoma-derived exosomes. (**E**) Confocal microscopy of MoDC from tumor-bearing mice incubated overnight with exosomes (x400). Graph (**F**) and confocal microscopy (**G**) of Caspase 3/7 activity in MoDC treated with B16F10 exosomes (n=3). (**H**) Confocal microscopy of MoDC isolated from WT or NLRP3 KO mice treated with B16F10 exosomes or activated $CD8^+$ T cells lysosomes. (**I**) Caspase 3/7 activity in MoDC

isolated from NLRP3 KO mice with or without B16F10 exosomes. (**J**) Tumor size (mm^2) in mice injected s.c. with YUMM1.7 cells and treated intratumorally with anti-TRP1 antibodies plus CD40L and TNFα (n=4). Shown is one experiment out of at least three performed. Statistical significance was calculated using ANOVA with Tukey's correction for multiple comparisons (*** denotes p<0.001, **** denotes p<0.0001).

Fig. 5: Tumor-infiltrating MoDC are required to license the cytotoxic activity of $CD8^+$ T cells- (**A**) Confocal microscopy of $CD8^+$ T cells isolated from tumor-bearing mice and co-cultured overnight with wasabi-labeled B16F10 melanoma cells (x200). (**B**) Mean percentages of B16F10 melanoma cells stained for Annexin V/PI (n=3). **(C)** Mean percentages of membrane-bound CD107a in $CD8^+$ T cells from tumor-bearing mice cultured overnight with B16F10 cells (n=3). (**D**) Confocal microscopy of DC and $CD8^+$ T cells from tumor-bearing mice incubated overnight with B16F10 melanoma cells (x200). (**E**) Mean percentages of B16F10 melanoma cells stained with Annexin V/PI following overnight incubation with $CD8^+$ T cells from the DLN of tumor-bearing mice (n=3). **(F)** Mean percentages of membrane-bound CD107a in $CD8^+$ T cells from the DLN of tumor-bearing mice (n=3). **(G)** Mean percentages of B16F10 melanoma cells stained with Annexin V/PI following overnight incubation with $CD8^+$ T cells from tumor-bearing mice (n=3). **(H)** Mean percentages of membrane-bound CD107a in DLN $CD8^+$ T cells (n=3). (**I**) Mean percentages of membrane-bound CD107a in $CD8^+$ T cells from the DLN of tumor-bearing mice cultured overnight with DC in the presence of blocking antibodies for MHC-I (n=3). (**J**) Mean percentages of DC expressing $CD40^+CD86^+$ in day 8 tumor-bearing mice (n=3). (**K**) $CD40^+CD86^+$ expression on DC from day 8 tumor-bearing mice. (**L**) Mean percentages of B16F10 melanoma cells stained with Annexin V/PI following overnight incubation with DC and $CD8^+$ from tumor-bearing mice (n=3). **(M)** Mean percentages of membrane-bound CD107a in $CD8^+$ T cells from the DLN of tumor-bearing mice cultured overnight with DC and B16F10 cells (n=3). Shown is one representative experiment out of at least three performed. Statistical significance was calculated using ANOVA with Tukey's correction for multiple comparisons (*** denotes p<0.001, **** denotes p<0.0001).

Fig. 6: Tumor-infiltrating MoDC are required for $CD8^+$ T cells immunotherapy - (**A**) B16F10 tumor size in mice treated with adoptive transfer of gp100-reactive $CD8^+$ T cells in CD11c-DTR BM chimeric mice pre-injected with PBS, or with diphtheria toxin (n=5). (**B**) B16F10 tumor size in mice treated with adoptive transfer of gp100-reactive $CD8^+$ T cells, and anti-CCL2 antibodies (n=4). (**C**) B16F10 tumor size in mice treated with anti-TRP1 antibodies+anti-CD40 and TNFα, and with anti-CCL2 antibodies (n=4). (**D**) Confocal microscopy images of tumor MoDC isolated from untreated late-stage tumors, or from tumors treated with GM-CSF and anti-CD40 (x400). (**E**) Mean percentages of tumor $CD45^+$, Pan DC and MoDC following treatment with adoptive transfer of $CD8^+$ T cells and anti-CD40 at late-stage. (**F**) B16F10 tumor size in mice treated with adoptive transfer of gp100-reactive $CD8^+$ T cells alone or with agonistic anti-CD40 and GM-CSF (n=4). Shown is one representative experiment out of at least three performed. Statistical significance was calculated using ANOVA with Tukey's correction for multiple comparisons (* denotes p<0.05, ** denotes p<0.01, **** denotes p<0.0001).

Fig. 7: Human melanomas induce cell death of MoDC and correlate with poor clinical outcomes. **(A)** Heatmap analysis of melanoma patients based on their expression profile of 16 genes indicative of activated MoDC. **(B)** Kaplan-Meier survival probability plot of melanoma patients clustered by expression profile of activated MoDC genes. **(C)** Annexin V/PI staining of tumor cells isolated from melanoma patient and incubated overnight with autologous T cells and tumor-infiltrating MoDC. (**D**)

Confocal microscopy images of tumor cells isolated from melanoma patient incubated overnight with autologous PB T cells, and with autologous tumor-infiltrating MoDC (x200). **(E)** Histological staining of cleaved caspase 3 in a PD-1 resistant melanoma patient. Confocal microscopy images (**F**) and caspase-3/7 activity (**G**) of human MoDC from a healthy donor incubated with exosomes isolated from A375 human melanoma cells. Statistical significance was calculated using ANOVA with Tukey's correction for multiple comparisons (** denotes $p<0.01$, *** denotes $p<0.001$).

Author Manuscript Published OnlineFirst on March 3, 2020; DOI: 10.1158/0008-5472.CAN-19-2944
Author manuscripts have been peer reviewed and accepted for publication but have not yet been edited.

Figure 1

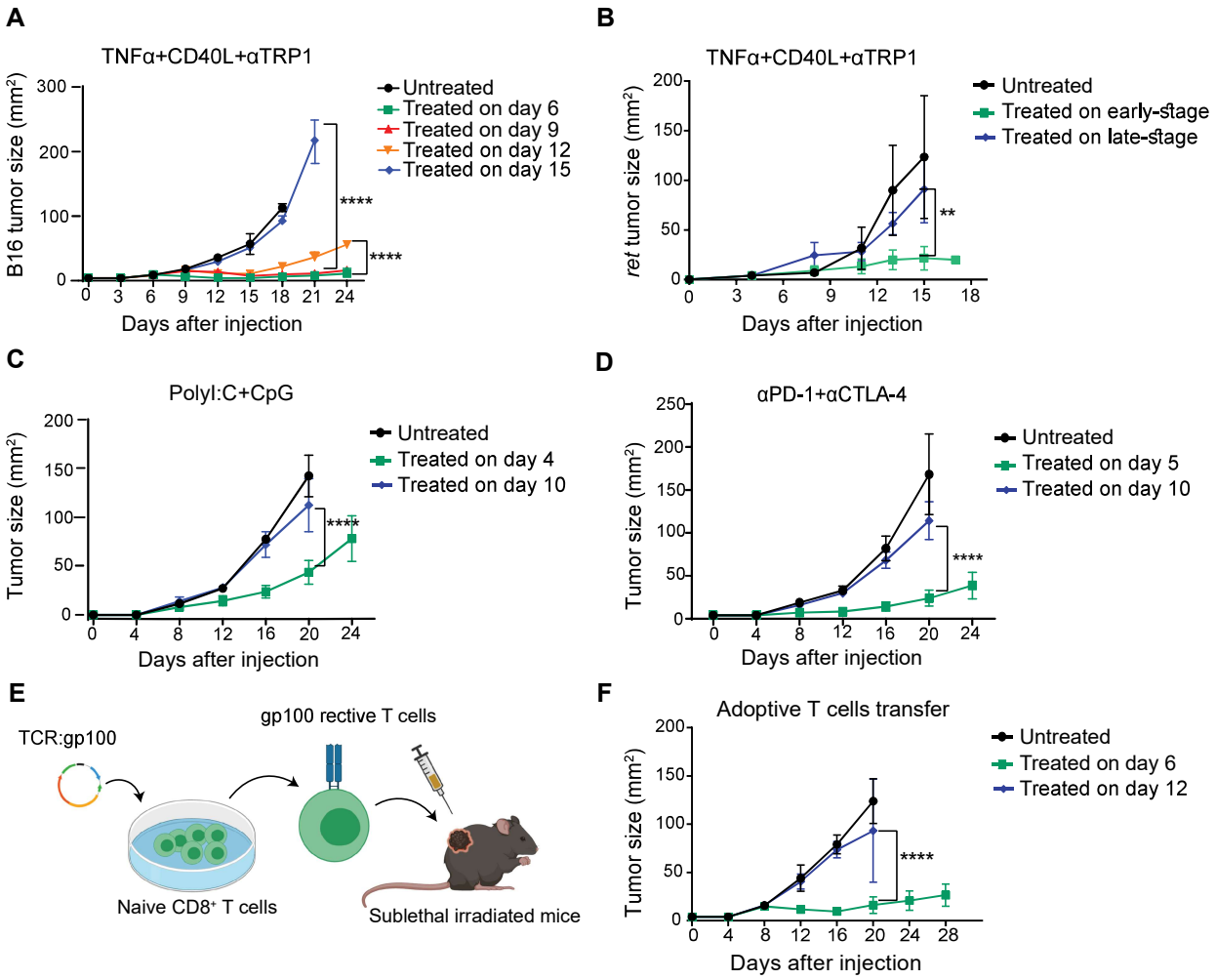

Author Manuscript Published OnlineFirst on March 3, 2020; DOI: 10.1158/0008-5472.CAN-19-2944
Author manuscripts have been peer reviewed and accepted for publication but have not yet been edited.

Figure 2

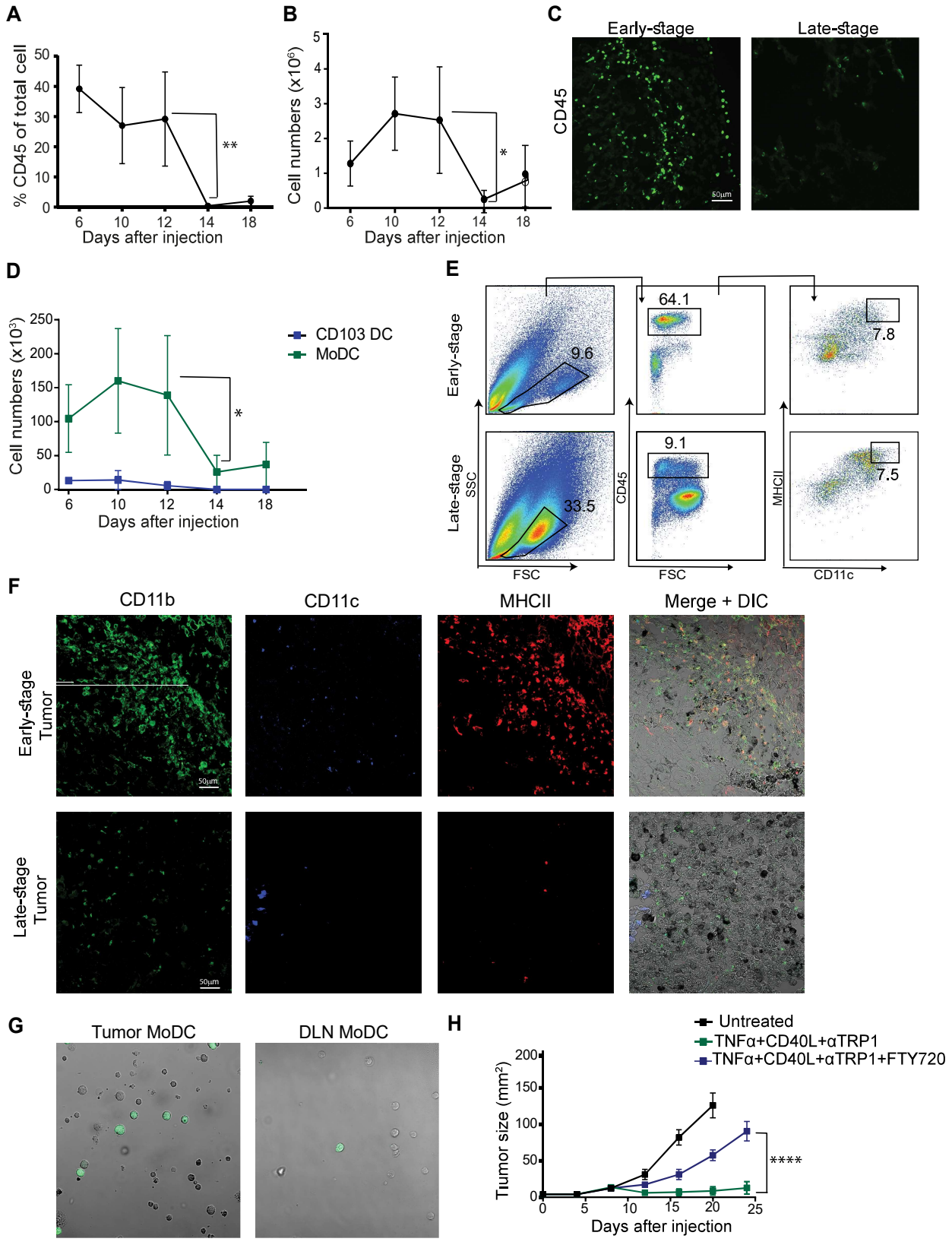

Figure 3

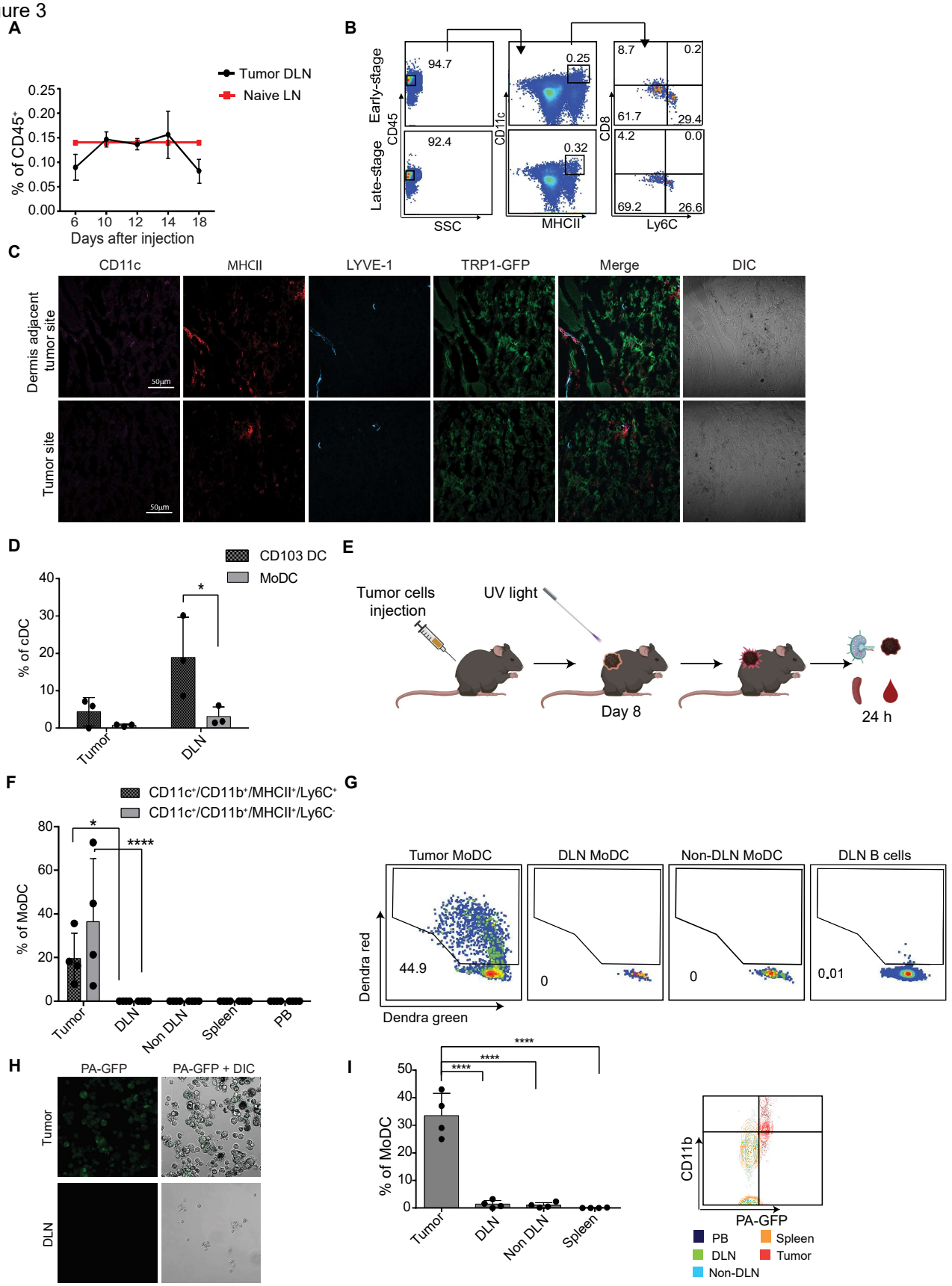

Author Manuscript Published OnlineFirst on March 3, 2020; DOI: 10.1158/0008-5472.CAN-19-2944
Author manuscripts have been peer reviewed and accepted for publication but have not yet been edited.

Figure 4

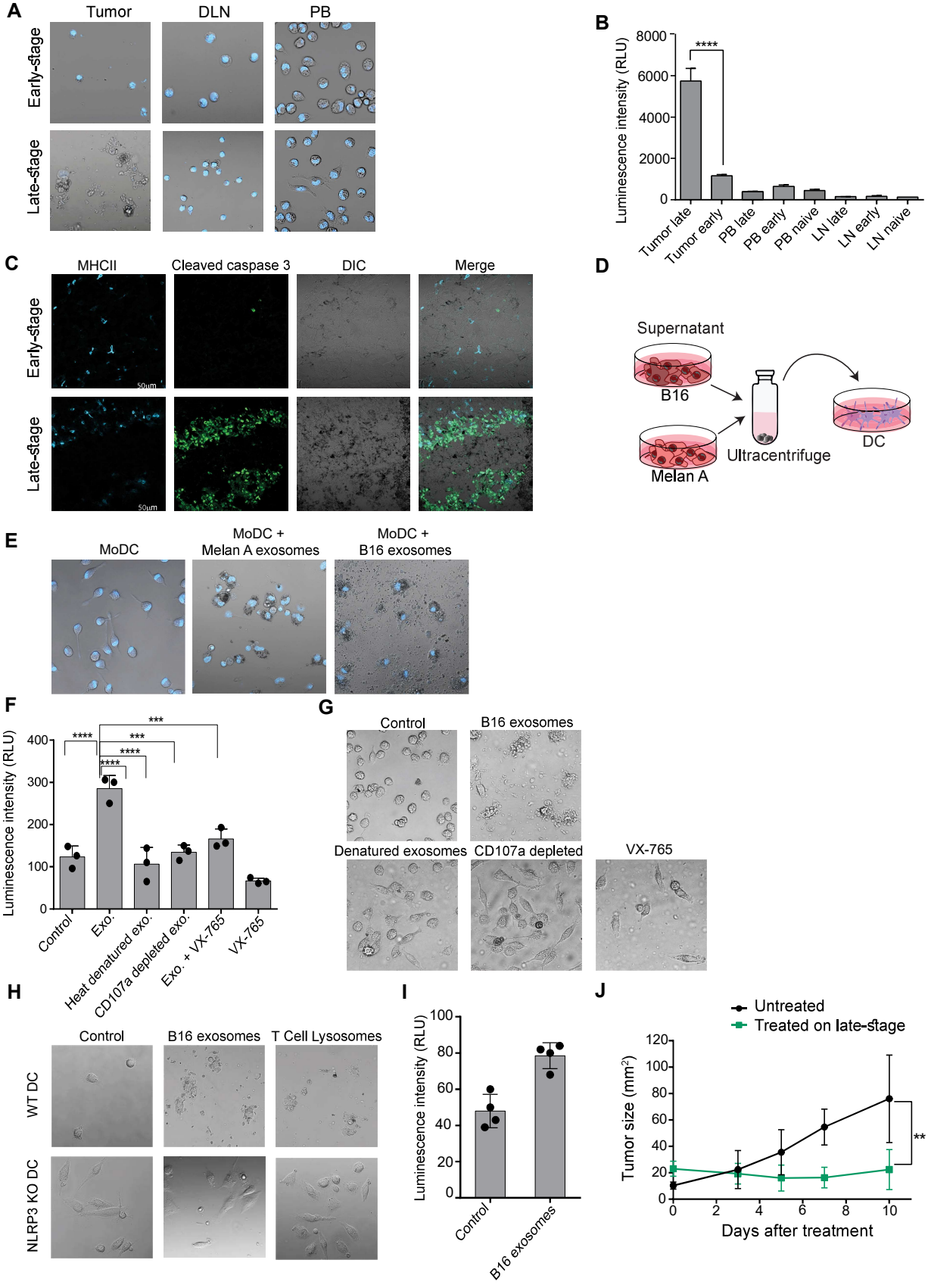

Author Manuscript Published OnlineFirst on March 3, 2020; DOI: 10.1158/0008-5472.CAN-19-2944
Author manuscripts have been peer reviewed and accepted for publication but have not yet been edited.

Figure 5

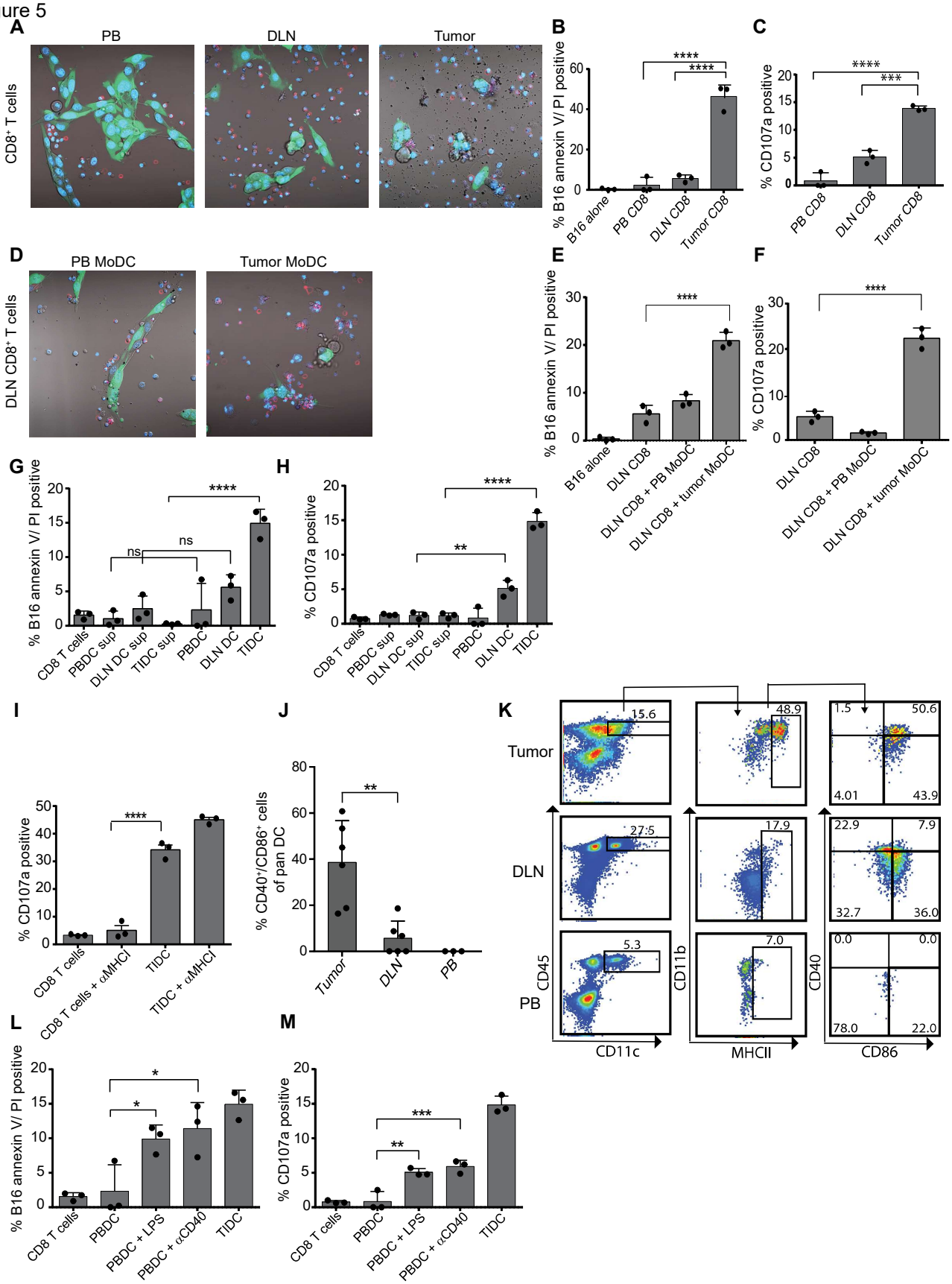

Author Manuscript Published OnlineFirst on March 3, 2020; DOI: 10.1158/0008-5472.CAN-19-2944
Author manuscripts have been peer reviewed and accepted for publication but have not yet been edited.

Figure 6

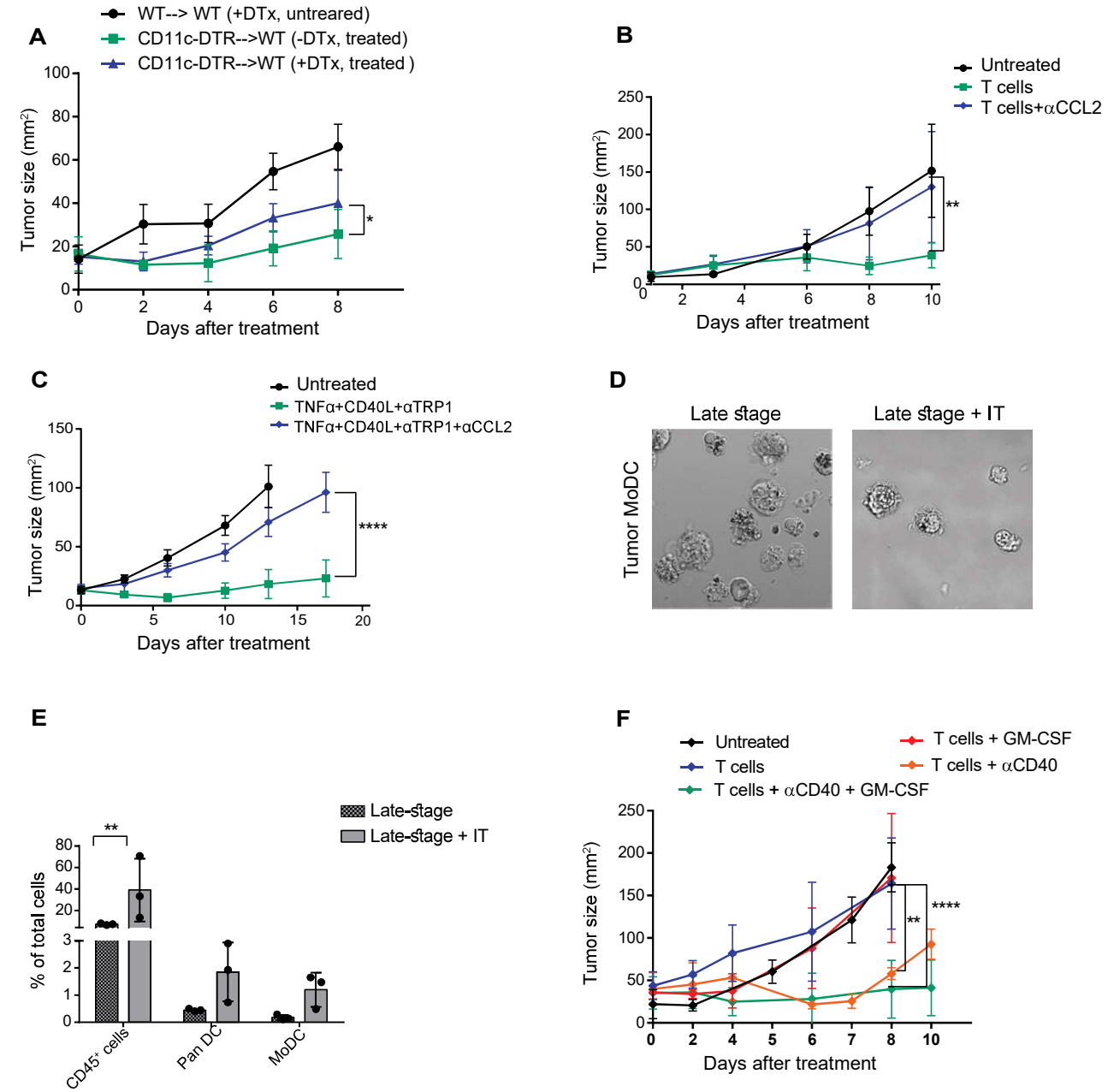

Author Manuscript Published OnlineFirst on March 3, 2020; DOI: 10.1158/0008-5472.CAN-19-2944
Author manuscripts have been peer reviewed and accepted for publication but have not yet been edited.

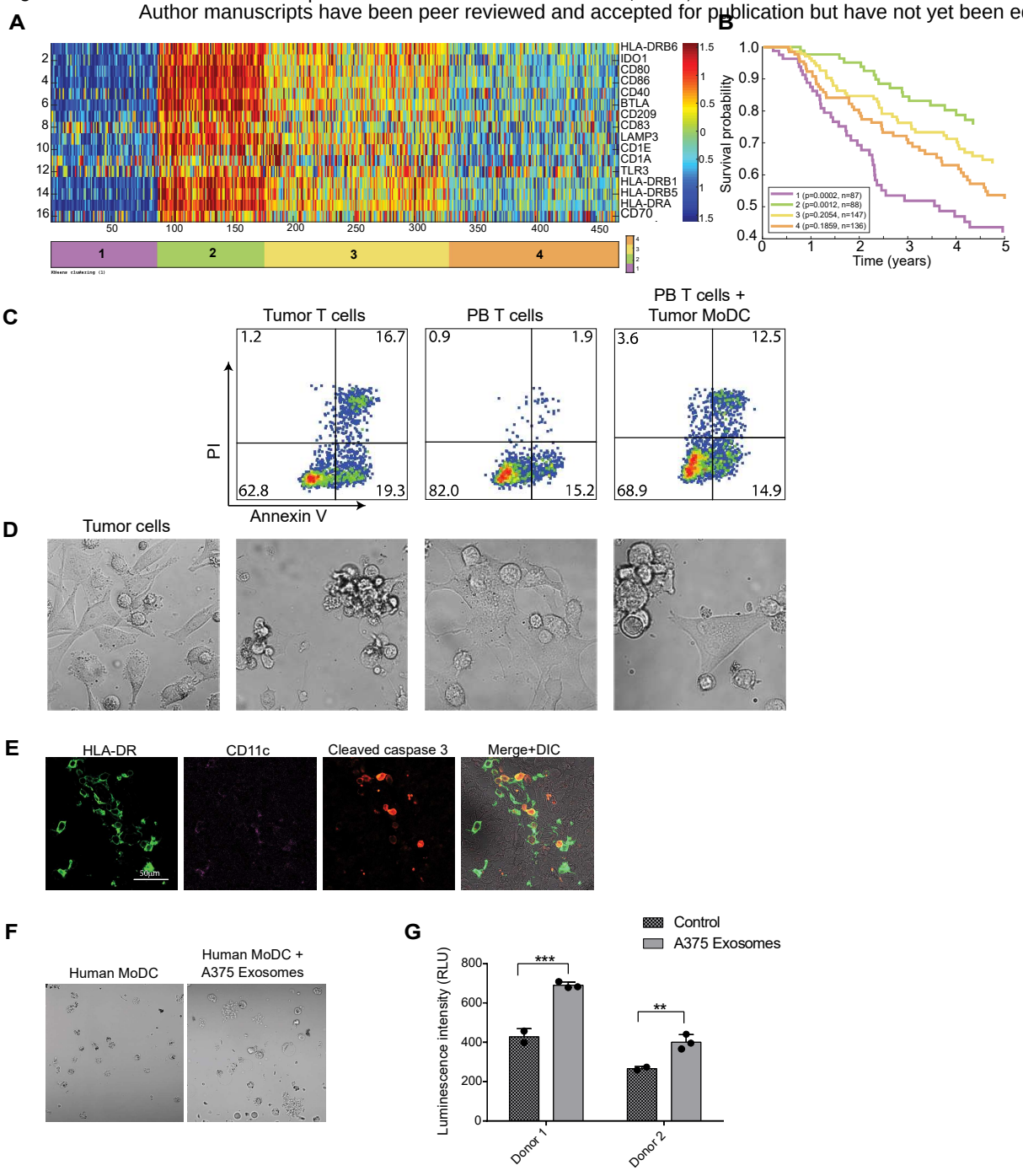

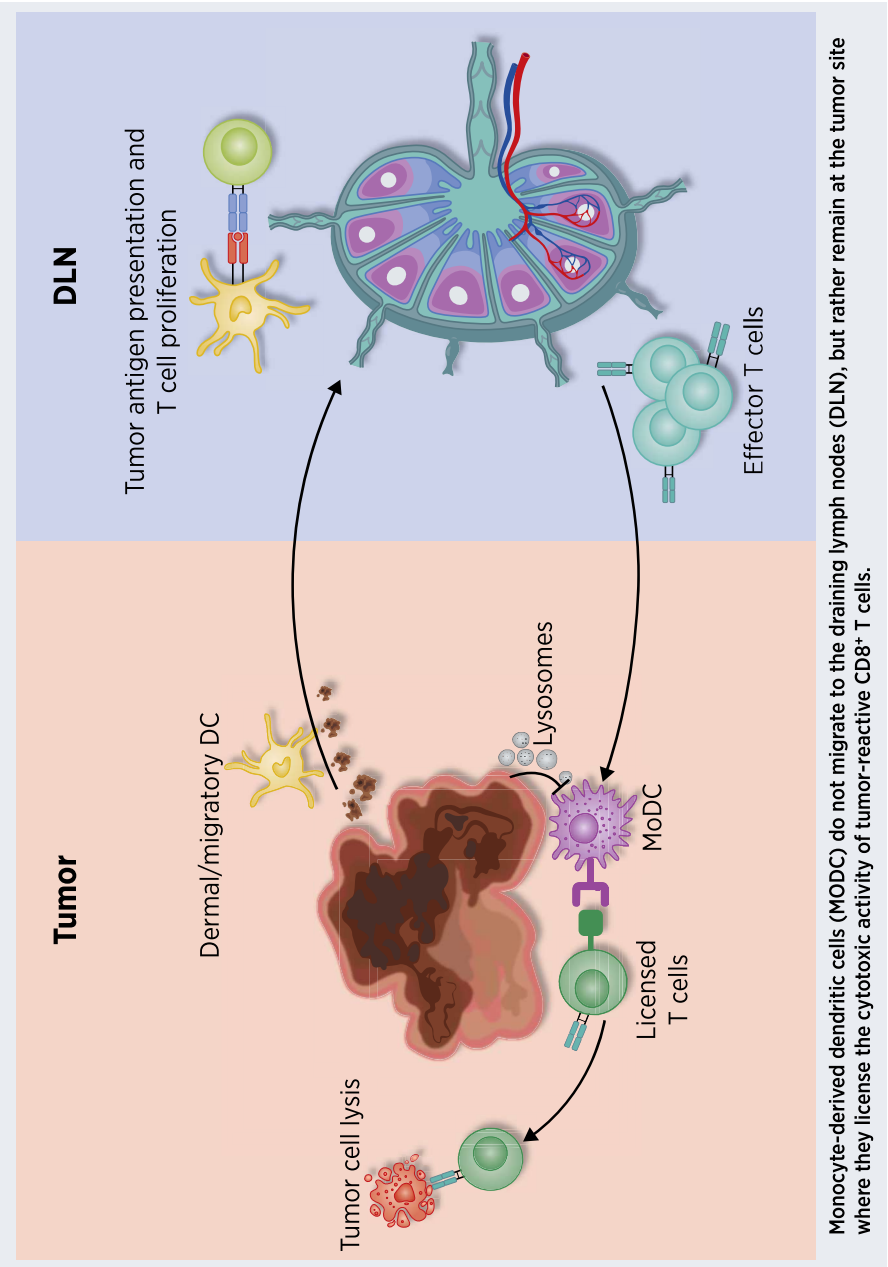

Monocyte-derived dendritic cells (MODC) do not migrate to the draining lymph nodes (DLN), but rather remain at the tumor site where they license the cytotoxic activity of tumor-reactive $CD8^+$ T cells.

AACR American Association for Cancer Research

Cancer Research

The Journal of Cancer Research (1916–1930) | The American Journal of Cancer (1931–1940)

Melanoma-secreted lysosomes trigger monocyte-derived dendritic cell apoptosis and limit cancer immunotherapy

Nadine Santana-Magal, Leen Farhat-Younis, Amit Gutwillig, et al.

Cancer Res Published OnlineFirst March 3, 2020.